

Novel Testing and Characterisation of High Modulus GFRP Bars in Compression

O.S. AlAjarmeh¹, A.C. Manalo^{1,*}, B. Benmokrane², PV Vijay³, W. Ferdous¹, and P. Mendis⁴

¹University of Southern Queensland, Centre for Future Materials (CFM), School of Civil Engineering and Surveying, Toowoomba 4350, Australia.

*Corresponding Author: manalo@usq.edu.au

²University of Sherbrooke, Department of Civil Engineering, Sherbrooke, Quebec, Canada

³Department of Civil and Environmental Engineering West Virginia University, Morgantown, WV 26506

⁴The University of Melbourne, Department of Infrastructure Engineering, Victoria 3010, Australia

ABSTRACT

Glass fibre reinforced polymer (GFRP) bars have now been increasingly used as longitudinal reinforcement in concrete columns. In column design and analysis, the contribution of GFRP bars to compression is often ignored or is estimated as a fraction of its tensile strength due to the limited understanding on their compressive behaviour. Moreover, there exists no standard test method to characterise the properties of GFRP bars in compression. This study implemented a novel test method to determine and characterise the compressive properties of high modulus GFRP bars. During the preparation of test specimens, hollow steel caps filled with cementitious grout were used to confine the top and bottom ends of the GFRP bars. The effects of the bar diameter (9.5, 15.9, and 19.1 mm) and the unbraced length-to-bar diameter ratio, L_u/d_b (2, 4, 8, and 16) were investigated on the compressive strength of the bars. The results showed that the increase in bar diameter increases the micro-fibre buckling and decreases the compressive-to-tensile strength ratio. Similarly, the failure mode changed from crushing to fibre buckling with the increase of L_u/d_b ratio. Simplified theoretical equations were proposed to reliably describe the compressive behaviour of GFRP bars with different bar diameters and L_u/d_b ratios.

Keywords: compressive test; GFRP bars; slenderness ratio; bar diameter; micro-fibre buckling; crushing.

INTRODUCTION

Glass Fibre Reinforced Polymer (GFRP) bars have been an effective alternative replacement to steel bars as internal reinforcement for concrete structures exposed to harsh environments due to their high strength and non-corrosive properties [1]. Investigation on concrete structures longitudinally and transversely reinforced with GFRP bars showed satisfactory performance in bending and shear [2-6]. Moreover, many experimental studies were conducted to characterise the mechanical [7-13], physical [14], chemical [15-17], thermal [8, 11, 18] and durability properties [10-11] of this type of reinforcements. These important properties have now been specified in CSA S807 [19] and ASTM D7957 materials specifications and design codes to ensure the quality, proper design, and safety of these reinforcing materials for their effective utilization as structural reinforcement. As a result, many GFRP reinforced concrete structures have been constructed including bridges [16], highway barriers, boat ramps planks [20], and concrete pavements [21] in aggressive environments.

In recent years, there is an increased interest in the use of GFRP bars as longitudinal reinforcement for concrete columns. A number of studies have shown the effectiveness of using GFRP bars for solid and hollow concrete columns [2-4, 31-34]. These studies emphasised the linear elastic response until failure of the GFRP bars as internal reinforcement in concrete columns. Moreover, Maranan et al. [2] stated that the compressive strength of 15.9 mm diameter GFRP bar is only 51.7% of its tensile strength with an equal elastic modulus, and will fail by buckling when the spacing between lateral spirals is 200 mm or more. Furthermore, AlAjarmeh et al. [3] investigated the compressive behaviour of the 12.7 mm, 15.9 mm, and 19.1 mm diameter GFRP bars in concrete columns with a spiral spacing of 100 mm. Consistent with Maranan et al. [2], all GFRP bars failed by crushing with the lower spiral spacing. These results indicated that the unsupported length has a major effect on the compression behaviour of GFRP bars, and requires a more detailed investigation.

The required testing and characterisation of GFRP bars to ensure quality and performance of the product are specified in a number of test standards [19, 22, 23]. The ASTM D695 [24] on the other hand is usually referred when evaluating the compressive properties of rigid plastics; however, the standard is not applicable to round GFRP bars. As there is still no standard procedure for testing and characterising the compressive properties of GFRP bars due to the variation of its behaviour under compression and also the obtained failure modes, the contribution of the GFRP bars is often ignored in the design and analysis of reinforced concrete columns. The main reason behind that is the non-homogeneity and the anisotropic nature of the GFRP reinforcements, where the shear and transverse tensile forces have significant influence on their compressive behaviour [25]. In most cases, the compressive strength of GFRP bars is reported as a fraction of their tensile strength. There is therefore a need to develop a new approach for testing and characterising the compressive behaviour of GFRP bars in order to advance their application as longitudinal reinforcement in concrete columns.

Some of the attempts to evaluate the compressive strength of GFRP bars are described by researchers [14, 26-30]. Chaallal and Benmokrane [28] investigated the compressive strength for three different diameters (15.9, 19.1, and 25.4 mm) of GFRP bars with a tensile elastic modulus of 42 MPa, and a slenderness ratio of 11 following ASTM D695-91 [23]. Their results revealed that the compressive strength of the GFRP bars was around 77% of the tensile strength and with the same modulus of elasticity in tension. Deitz et al. [14] studied the effect of slenderness ratio on 15 mm diameter (177 mm^2) GFRP bars with tensile strength and Young's modulus of 610 MPa and 40 GPa, respectively, using a modified ASTM D695-10 test procedure [24]. Three replicates for each slenderness ratio (ranging from 3.3 to 25.3) were tested. They found that the GFRP bars can fail in three modes, i.e. (1) crushing for bars with slenderness ratio less than 3.3, (2) buckling for bars with slenderness ratio more than 14, and (3) combined buckling-crushing for bars with an unbraced length between 3.3 and 14. In

another study, the bars with a low slenderness ratio exhibited compressive strength of only 50% of their tensile strength with a fibre fraction content of 70% [31]. The compressive strength further decreased with an increase in the slenderness ratio. They also observed a similar modulus of elasticity in tension and compression for bars with same slenderness ratio. On the other hand, Bruun [30] investigated the relationship between compressive strength and the unbraced length ranging from 50 mm to 600 mm by testing 25 mm diameter GFRP bars. Two replicates for each unbraced length were tested. They indicated that the compressive strength of up to 730 MPa could be reached when the clear height is less than 230 mm and the failure mode was pure crushing. The compressive strength decreases with the increase of sample's clear height due to buckling effects. However, the tensile properties of the tested bars are not reported for comparison. Khan et al. [26] tested 15.9 mm diameter GFRP bars in tension and compression, with a slenderness ratio of 5 for compression. Based on the testing of three bars in tension and five bars in compression, they obtained an average compressive strength of only 61% of the tensile strength and a modulus of elasticity 33% lower than the tensile modulus. Premature splitting at top and bottom of bars was also observed at the unrestrained ends. More recently, three groups of five GFRP bars samples were tested in compression using a method suggested by Khorramian and Sadeghian [27, 32] and Fillmore and Sadeghian [33]. Different bar diameters of 19.1, 15.9, and 13.0 mm with slenderness ratio of 2 were tested. The top and bottom portion of the bars were embedded into hollow steel caps (32 in diameter and 12.7 in height) filled with epoxy-based adhesives. The tested GFRP bars showed an inclined crushing failure. The ratio between the compressive and tensile strength and the strain ranged between 0.74-1.00 and 0.58-0.82, respectively, with the compressive and tensile elastic moduli having similar values. Khorramian and Sadeghian [34] recently summarise those attempts [27, 32, 33] by suggesting a new testing methodology for determining the compressive behaviour of the GFRP bars.

From these earlier studies, it is clear that there are inconsistencies between results from the different compressive tests conducted on GFRP bars. Moreover, no generalisations can be made about the results as different researchers used either only limited number of specimens or a single bar diameter or a specific slenderness ratio. Further research in this regard and a more systematic approach is therefore needed to clearly examine the compressive behaviour of GFRP bars.

This study comprehensively investigates the compressive behaviour of high modulus GFRP bars using a novel test procedure. Three unbraced length/bar diameter (L_u/d_b) ratios and three bar diameters were considered, and their effect on the compressive behaviour of GFRP bars was determined, thus providing a direct comparison of the important properties. The outcome of this study will contribute to a more detailed understanding on the compressive behaviour of GFRP bars and will provide useful information to design engineers seeking to make an informed and justifiable decision about the use of GFRP bars as an internal reinforcement in concrete columns. Furthermore, the results of this study may prompt researchers and manufacturers to develop innovative new test procedures and materials specifications to ensure the quality of GFRP reinforcements.

TESTING PROGRAM

Physical and Tensile Mechanical Properties of GFRP Bars

Three high-modulus (Grade III) GFRP bars with a nominal diameter of 9.5, 15.9, and 19.1 mm were considered in this study (see Figure 1). High-modulus GFRP bars were selected due to their effectiveness as longitudinal reinforcement and significant load contribution in concrete columns [2-4]. The bars contain glass fibres which were impregnated with vinyl-ester resin using pultrusion process. The outer surface of GFRP bars was coated with sand particles. All GFRP bars were manufactured at the same time and came from the same production lot as

tested by Benmokrane et al. [15]. The physical and tensile-related mechanical properties of the GFRP bars are listed in Table 1, with the mechanical properties calculated based on the nominal area, as suggested by the CSA-12 [19]. Standard deviation of the results is provided within parenthesis.

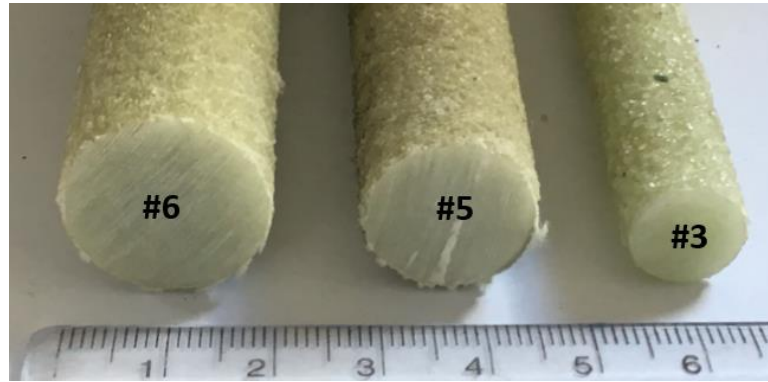


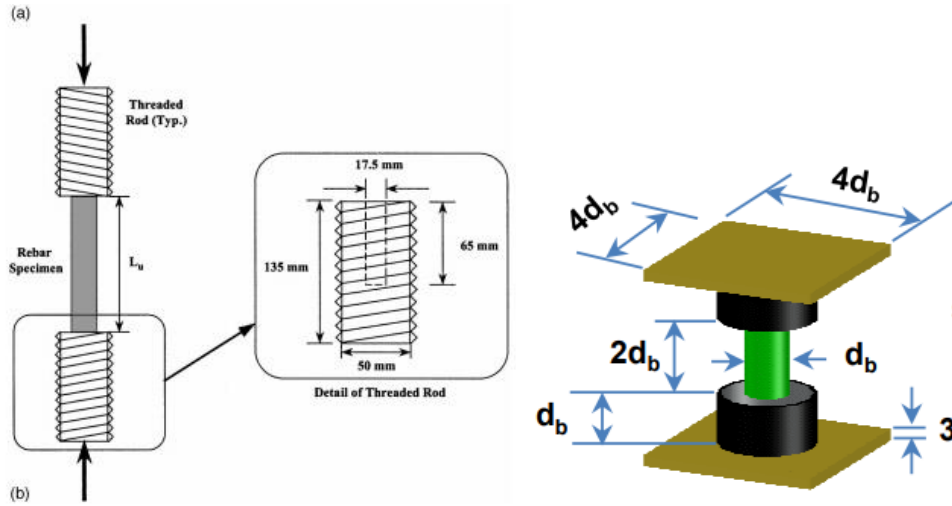
Figure 1. Considered GFRP bars

Table 1. Physical and mechanical properties of the GFRP bars

	Properties	Test Method	Number of Samples	Bar grade		
				#6	#5	#3
Physical properties	Nominal bar diameter (mm)	CSA S806, Annex A [34]	9	19.1	15.9	9.5
	Nominal bar area (mm ²)	CSA S806, Annex A [34]	9	286.5	198.5	70.8
	Actual bar area (mm ²)			(1.9)	(1.2)	(1.9)
	Fiber content by weight (%)	ASTM D3171–15 [35]		80.9 (0.2)	82.6 (0.1)	82.7 (0.2)
Mechanical properties	Ultimate tensile strength, f_{fu} (MPa)	ASTM D7205/D7205M-06 [36]	6	1270.0 (31.4)	1237.4 (33.3)	1315.0 (31.1)
	Modulus of Elasticity, E_{fu} (GPa)	ASTM D7205/D7205M-06 [36]	6	60.5 (0.5)	60.0 (1.3)	62.5 (0.4)
	Ultimate strain, ϵ_u (%)	ASTM D7205/D7205M-06 [36]	6	2.1 (0.1)	2.1 (0.1)	2.3 (0.1)

New Procedure for Compression Testing of GFRP Bars

The compressive properties of GFRP bars are important and necessary when used as longitudinal reinforcement in concrete structures. Identifying the structural behaviour of GFRP bars requires the knowledge of possible failure modes and their strength limits for a safe and reliable design. However, there exists no materials' specifications nor test standards in identifying the compressive behaviour of GFRP bars. A few researchers [28] tested GFRP bars in compression following the ASTM D695 test procedure where premature splitting was observed due to high-stress concentration at the ends which propagated through the entire length of the bars. Some attempts [14, 30] were made to modify the ASTM D695 procedure (Figure 2a) by inserting the bar ends in a steel rod. Due to the fixed end conditions created by the stiff steel rods, the bar sample was cut vertically at the contact point of the bar sample and the steel rod after a splitting failure. This occurrence was due to the significant difference between the transverse stiffness of the GFRP bars and the stiffness of the steel rod. Moreover, the test results cannot be generalised as the number of samples were very limited and had a significant variation between them [14, 30]. While the test method suggested by Khorramian and Sadeghian [27, 32] and Fillmore and Sadeghian [33] shown in Figure 2b can provide a consistent compressive strength of GFRP bars by sealing the bar ends with epoxy resin. However, it was captured [37] that many samples showed crushing failure at the bar ends within the epoxy-sealed zone due to the softening behaviour of the epoxy resin which could not confine the ends very well. On the other hand, the sealed ends at the top and bottom steel caps made the removal of the tested bars difficult and their reuse unsuitable for next specimen preparation or testing. Similarly, this method was implemented only for testing relatively short GFRP bar samples.



(a) Deitz et al. [14]

(b) Khorramian and Sadeghian [27, 32]

Figure 2. Available test method for compression test of GFRP bars

In this study, a new test procedure involving preparation of the GFRP bar samples with capping at top and bottom ends enabled plumb-positioning of the specimens within the test machine and concentric load application. This method is similar to that of Khorramian and Sadeghian [29, 34] and Fillmore and Sadeghian [35] but without the sealed ends allowing easy removal of the failed samples and reuse of the steel tubes for the next specimen preparation. Moreover, the use of two heavy thick steel plates was eliminated, which if present, could potentially affect the measured strength of the bars. This approach is also similar to the compressive test method proposed by Manalo et al. [38] wherein the top and bottom ends of the thick composite laminates were steel capped to minimise stress concentration at the load application zones and to promote a failure within the unsupported length.

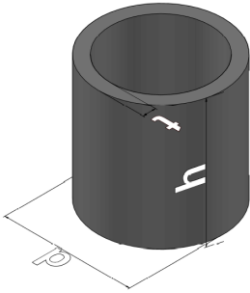
In the preparation of the test specimens, the diameter and thickness of the steel pipes for the end caps were based on the recommendation from ASTM D7205/D7205M-06 [39] for tensile tests of GFRP bars. Both ends of the GFRP bars were inserted into steel tubes with a cement grout filling the gap between them. Expansive cement grout (with characteristic compressive strength of 60 MPa) was used to confine the lateral expansion of the top and

bottom ends of the GFRP bars under compression load. The steel pipes were prepared with a height-to-diameter ratio of 1:1 to provide the confinement but facilitate the easy removal of the bar after the testing. This approach also mimics the semi-fixed (close to the pinned-end case) boundary conditions [40-43] provided by the lateral ties to the longitudinal bars in concrete columns. Figure 3 shows the three adopted caps in this study, and Table 2 lists the cap dimensions.



Figure 3. Hollow steel sections (caps)

Table 2. Dimensions of the steel caps

	Bar diameter, d_b (mm)	9.5	15.9	19.1
	Outer Diameter, d (mm)	33.7	42.4	48.3
	Wall thickness, t (mm)	4.0	4.0	4.0
	Height, h (mm)	35	42	48

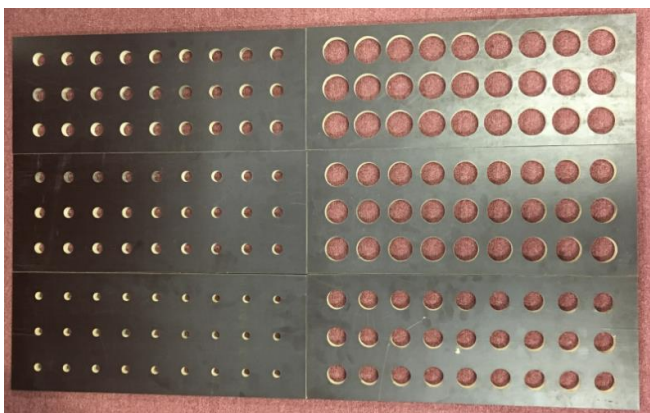
Test Matrix and Specimen Fabrication

The GFRP bar samples for compressive tests were designed and prepared to have different unbraced lengths, where the unbraced bar lengths (L_u) is the clear length between two steel caps (Figure 4). Four L_u/d_b ratios (2, 4, 8, and 16) covering the range of those investigated by previous researchers were considered, where d_b is the bar diameter. Six number (N) of replicates were prepared for each L_u/d_b ratio as per ASTM D7205/D7205M-06 [39] for

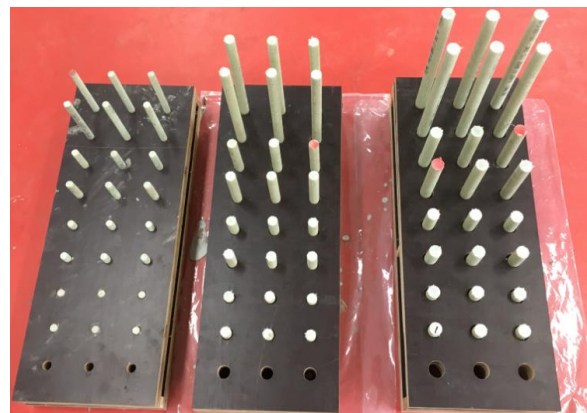
satisfying the minimum number of specimens for tensile testing of GFRP bars. It is worth noting that the CSA S807-10 [44] recommends only 5 duplications for the tensile test. Table 3 provides the unbraced length (L_u) and the total length (L_T) in mm of the test specimens. For test specimen preparation and fabrication, plywoods planks were drilled with concentric holes of required diameter (with a tolerance of ± 0.5 mm) (see Figure 4a) to hold the steel tube into position and properly align the GFRP bars (see Figure 4b), which is a very important step to ensure that the bars are subjected to pure compression by eliminating bending related to potential eccentricity in load application. Figures 4c and 4d show the test samples with top and bottom caps, and schematic diagram of a test specimen, respectively. The samples were named by the bar number first followed by the L_u/d_b ratio and then the sample number. For example, 5-16-3 is a #5 GFRP bar (15.9 mm diameter) with L_u/d_b ratio of 16 and a sample number of 3.

Table 3. Sample design matrix

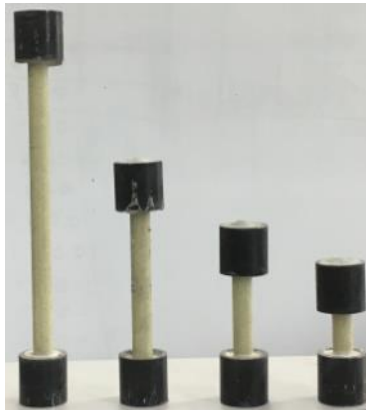
Bar number	d_b (mm)	$2d_b$		$4d_b$		$8d_b$		$16d_b$	
		L_u	L_T	L_u	L_T	L_u	L_T	L_u	L_T
#3	9.5	19.0	89.0	38.0	108.0	76.0	146.0	152.0	222.0
#5	15.9	31.8	115.8	63.6	147.6	127.2	211.2	254.4	338.4
#6	19.1	38.2	134.2	76.4	172.4	152.8	248.8	305.6	401.6



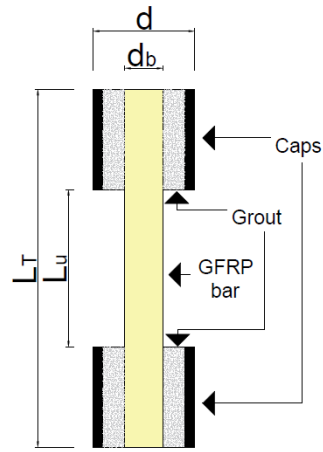
(a)



(b)



(c)



(d)

Figure 4. (a) Drilled plywood sheets for bars and caps (b) Fabricating bar samples in plywood moulds (c) Samples prepared for testing (d) schematic diagram of the test specimen

Instrumentation and Test Set-up

All samples were tested until failure under concentric compressive load using a SANS machine with the applied load measured using a 500 kN load cell (see Figure 5). Before commencing the test, strain gauge with a 3 mm gauge length was attached on opposite sides of the two of the tested GFRP bars at mid-height to capture the stress-strain behaviour. The applied load and strain data were recorded using a System 5000 data logger. As a safety precaution, the GFRP bars with L_u/d_b ratio of 8 and 16 were loosely strapped to the test machine as shown in Figures 6b and 6c to prevent dislodging, if any from the test machine after failure. It is noteworthy that the upper loading steel platen allowed the sample to have some end rotation indicating a pinned-end connection, which is an ideal behaviour for reinforcing bars under compression as suggested by other researchers [40-43]. The adopted displacement rate was 1.5 mm/min to produce the failure within 1 to 10 minutes after applying the load as recommended by ASTM D7205/D7205M-06 [36] for the tensile test of GFRP bars.

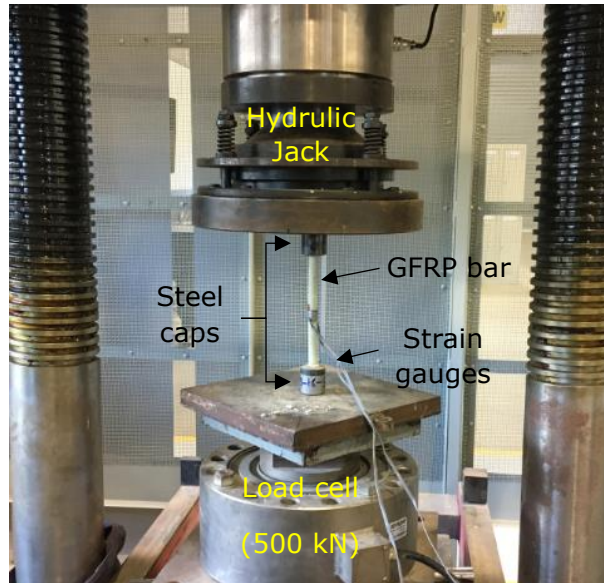


Figure 5. Set-up of compression test of GFRP bars

TEST RESULTS

Failure Modes

Three modes of failure such as crushing, buckling, and a combination of crushing and buckling (splitting) were observed in the GFRP bars tested in compression, which were highly influenced by the L_u/d_b ratio. More details of the observed mode of failure are described below:

Crushing Failure

Crushing failure mode was observed for bars with low L_u/d_b ratio (2 and 4), regardless of bar diameters. This failure is governed by shear as shown by the inclined crushing shear surface in Figures 6a to 6c. Similar mode of failure was observed by Khorramian and Sadeghian [32], and Fillmore and Sadeghian [27, 33] for GFRP bar samples with unbraced length-to-bar diameter ratio of 2. This mode of failure is however inconsistent to that of Dietz [14] and Bruun [30] wherein crushing of the whole bar length without any shear effect was noticed for the same L_u/d_b ratios, which might be related to the difference in the test setup. Some bars with $L_u/d_b = 2$ suffered from localised crushing either at the top- or bottom-end heads (see Figure 6d). This localised crushing is caused by the damage in the matrix due to high stress

concentration at the top and bottom ends of the bars which resulted in brooming of the fibres. This phenomena can be related to the weak strength of the GFRP bars in the transverse direction where the lateral expansion resistance is provided only by the matrix. Moreover, this behaviour can be also observed in the previous studies [14, 27, 30, 32, 33].

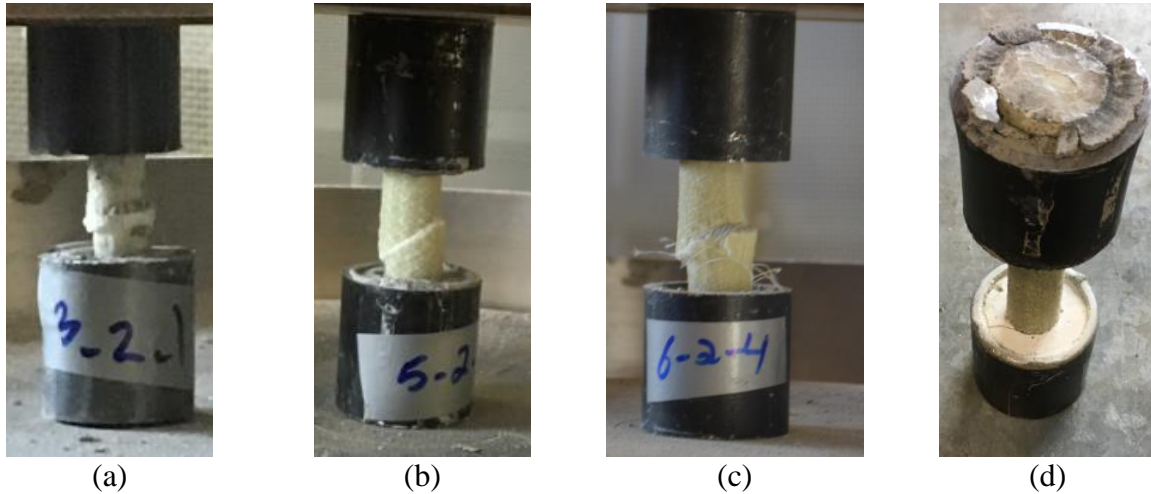


Figure 6. Mode of failure for bars with 2 and 4 L_u/d_b ratios for GFRP bar (a) #3 (b) #5 (c) #6 and (d) the premature failure.

Buckling Failure

Global buckling of the whole unbraced length was observed for all samples with L_u/d_b ratio of 16 regardless of the bar diameter (see Figures 7(a-c)). Similar findings were reported by Deitz [14] and Bruun [30] for GFRP bars with bar diameters of 15 mm and 25 mm, and L_u/d_b ratios of 14 and 12.6, respectively. After removing the applied loads, the failed samples returned to their original straightened positions but with the occurrence of few thin longitudinal splitting cracks at the outer surface (Figure 7d). The longitudinal cracks were caused by splitting between the fibers and the matrix due to the huge curvature under load.

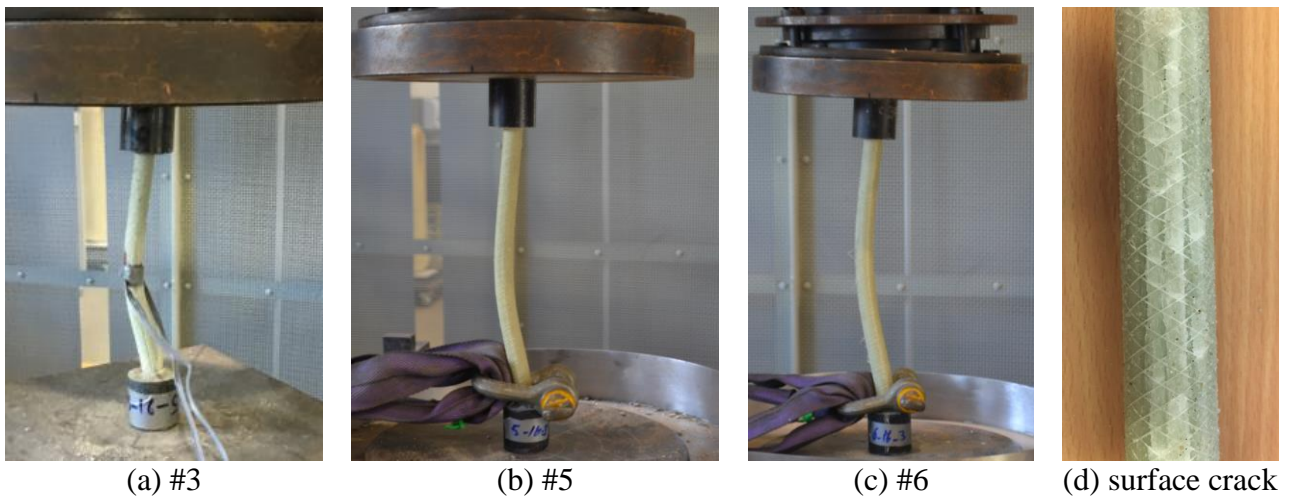


Figure 7. Mode of failure for GFRP bars with $L_u/d_b = 16$

Combination of Crushing and Buckling (Splitting)

The third mode of failure was a combination of crushing and buckling resulting in splitting between the fibres in addition to significant damage in the matrix as shown by separate bundles of the damaged GFRP bars (Figures 8a to 8c). This mode of failure was observed for all bars with $L_u/d_b = 8$. A similar mode of failure was observed by Bruun [30] for the samples with a bar diameter of 25 mm and L_u/d_b ratio less than 9.2, while Deitz [14] observed the same mode of failure for all tested samples with a bar diameter of 15 mm and L_u/d_b ratio less than 7.3. These damage and failure modes consisting of combined crushing and buckling leading to longitudinal matrix-fiber splitting are found to be related to the modulus of elasticity of the tested GFRP bars, which were 60.0 GPa and 42.5 GPa for the studies conducted by Bruun [30] and Ditez [14], respectively. It was also observed that the severity of the damage increased for the larger diameter bars. This observation might be due to higher load required for failing larger than smaller diameter GFRP bars which release high energy during failure due to their increased size.

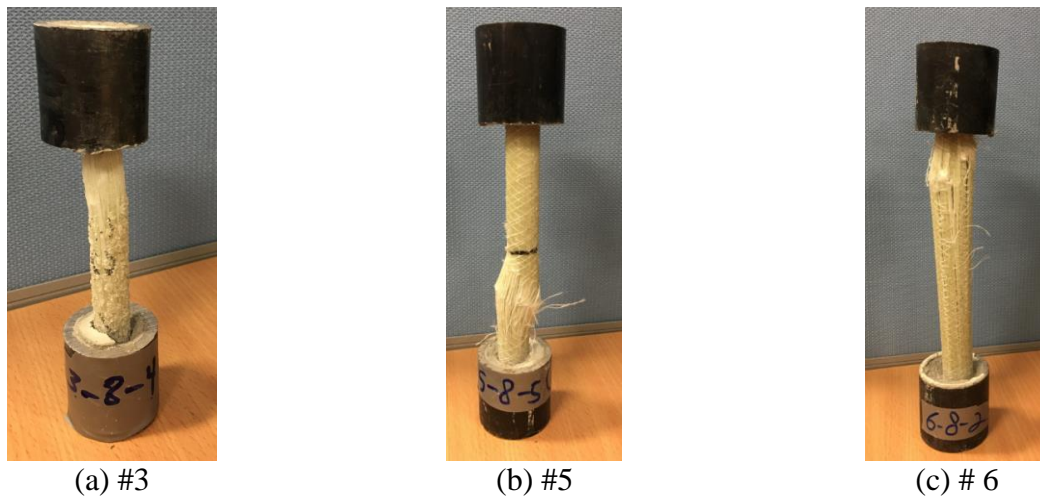
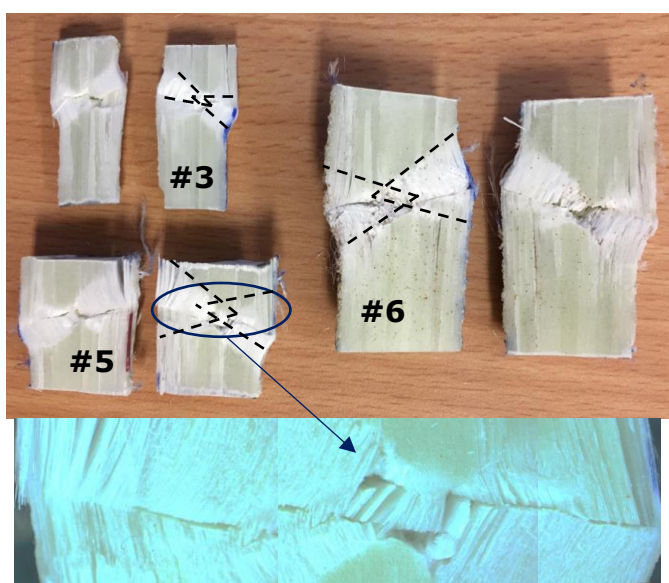
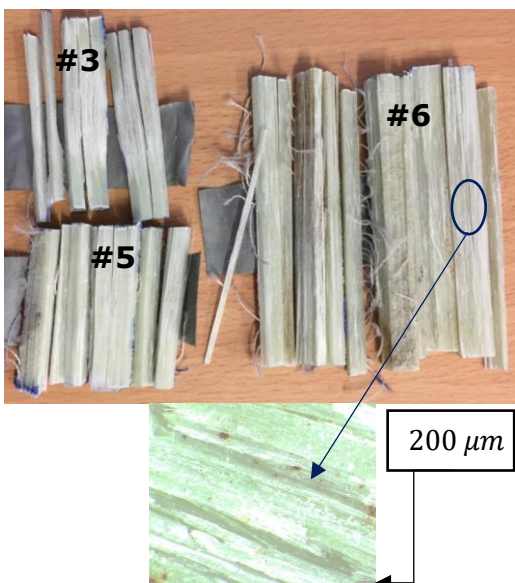
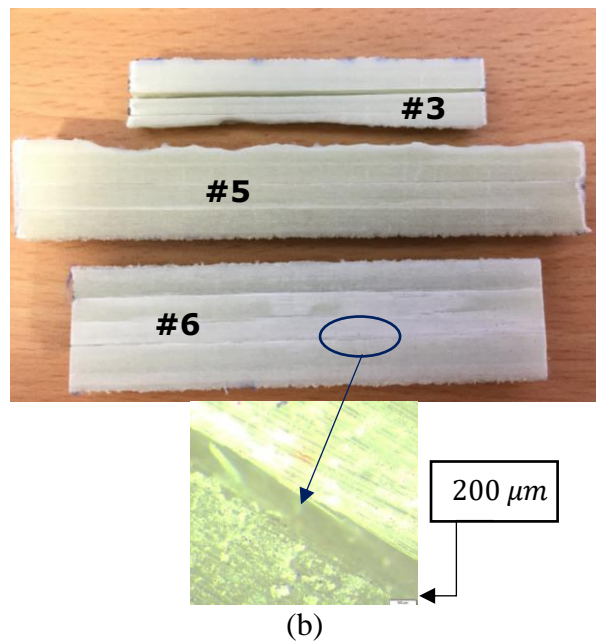
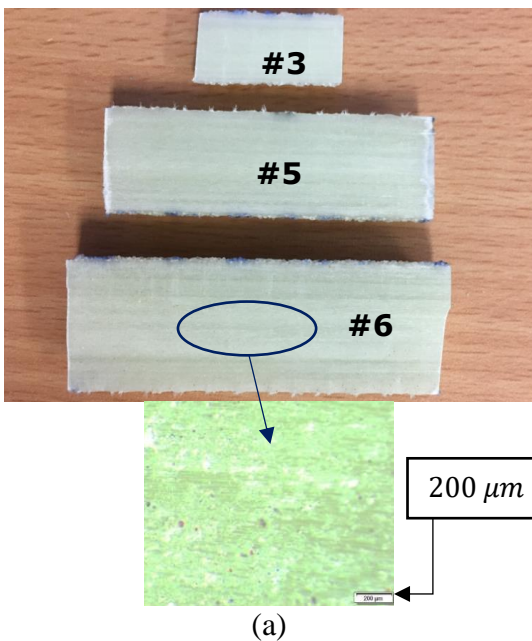


Figure 8. Mode of failure for GFRP bars with L_u/d_b of 8

Cross-Sectional Failure Investigation

The tested GFRP bars with different diameters were cut vertically using a water-jet for a detailed investigation of the failures along the longitudinal and diametrical cross-sections. An optical microscopic machine (Motic®) was used to observe the cross-sectional failure. The untested bar (Figure 9a) was used as a reference for comparing with the tested GFRP bars (see Figures 9b to 9d)). In Figure 9a, the cross-section of the untested bars was free of any cracks as evident by the homogenous and uniform texture of the cut surface. On the other hand, the bars which failed in buckling presented in Figure 8b show a few longitudinal cracks (between 3 to 5 cracks) in the matrix but without any damage to the fibres. Unlike the latter, the GFRP bars with $L_u/d_b = 8$ show an increased separation in the matrix with fibre fracture (Figure 9c). In fact, GFRP bars with $L_u/d_b = 8$ used for reinforcing concrete columns showed an identical mode of failure [2, 45], which demonstrates that bars with $L_u/d_b = 8$ represent closely the behaviour of the longitudinal reinforcing bars in actual concrete columns. On the contrary, the bars failed by crushing (Figure 9d) exhibited shear sliding wherein the outer fibres failed by micro-fibre buckling (kinking of the glass filaments resulting in a fracture at the mid-height of these filaments), and crushing of the fibres and matrix at the middle section of the bar. This failure behaviour indicates a non-uniform stress distribution along the cross-section of the

GFRP bars resulting in the outward fibre buckling. This tendency of the fibres to buckle is higher for bigger than smaller bar diameters wherein a more uniform and reduced intensity of fibre buckling was seen in the smaller diameter bars. This can be further illustrated by the two imaginary nested triangles, denoted by the dashed lines in Figure 9(d) formed at the boundary of the buckled glass fibres. It should also be mentioned that the crushed fibre and matrix at the centre of the bar was caused by the shear sliding of the outer kinked fibres. Some localised minor splitting cracks were also observed due to the extension of the micro-fibre buckling from the outer damaged zone to the inner crushed region.



(c)

(d)

Figure 9. The inner surface insight of GFRP bars for (a) un-tested samples, and different L_u/d_b ratio of (b) 2 and 4 (c) 8 (d) 16

Compressive Strength (f_{fc}) of GFRP Bars

Table 4 summarises the test results of the compressive strength (f_{fc}) for all tested GFRP bars.

The f_{fc} was calculated by dividing the maximum load with the nominal cross-sectional area of the GFRP bars listed in Table 1. In Table 4, test results generally show higher f_{fc} values for #3 bars compared to #5 and #6 bars. The maximum average f_{fc} value recorded for #3 bars is 1,319 MPa, while it is 899 MPa and 921 MPa for #5 and #6 bars, respectively. It can be noticed in Table 4 that f_{fc} values of #3 bars are almost equal to those bars with L_u/d_b ratio = 4 and 8, while it is significantly lower than that for #5 and #6 bars. Furthermore, a significant drop in f_{fc} values was measured for all bar diameters at L_u/d_b ratio = 16. On the other hand, the average f_{fc} values of #3 and #5 bars increases as the L_u/d_b ratio increases from 2 to 4 and 8. On the contrary, a clear convergence of f_{fc} values can be found for #6 bars. Noticeably, more consistent and convergent test results were observed for bigger than smaller diameter bars as evidenced by the lower standard deviation (SD) and coefficient of variation values. Similar trends can be noticed in the results of the #6 bars for increased L_u/d_b ratios.

Table 4. Compressive strength (f_{fc}) (MPa) of the tested GFRP bars with various L_u/d_b ratio

Sample number	#3 (9.5 mm) bar				#5 (15.9 mm) bar				#6 (19.1 mm) bar			
	L_u/d_b ratio				L_u/d_b ratio				L_u/d_b ratio			
	2	4	8	16	2	4	8	16	2	4	8	16
1	1215	1415	1333	519	960	831	902	345	761	933	818	349
2	1017	1613	1168	525	924	892	832	349	758	858	945	323
3	436	1430	1422	578	831	935	829	350	803	1089	959	363
4	546	989	1422	615	441	605	911	364	850	850	820	316
5	782	1242	1278	553	890	920	1009	390	991	869	802	334
6	871	1154	1290	574	1201	676	909	342	989	924	998	335
Average	811.1	1307.1	1319.0	560.7	874.5	809.9	898.6	356.8	858.7	920.6	890.5	336.5
SD	264.7	204.0	88.4	32.9	225.8	125.4	60.1	16.5	97.8	81.9	78.9	15.6
CoV (%)	32.6	15.6	6.7	5.9	25.8	15.5	6.7	4.6	11.4	8.9	8.9	4.6
(f_{fc}/f_{fu})\times100	61.7	99.4	100.3	42.6	70.7	65.4	72.6	28.8	67.6	72.5	70.1	26.5

Stress-Strain Behaviour

Figure 10 presents the typical stress-strain behaviour of GFRP bars with different L_u/d_b ratios. A linear elastic stress-strain behaviour was observed in GFRP bars with L_u/d_b ratio of 2 and 4 regardless of the bar diameter (Figures 10a to 10c). Moreover, an almost similar strain reading was measured by the strain gauges attached on both sides of the bars indicating that the load was applied concentrically and there was no bar buckling until failure. This stress-strain stability was observed up to failure of the bars that exhibited localised crushing (Figure 6a to 6c). Similar behaviour was noticed in previous studies [14, 32, 33] for GFRP bars having almost the same L_u/d_b ratios. On the other hand, GFRP bars with $L_u/d_b = 8$ (Figures 10d to 10f) exhibited a linear elastic stress and strain behaviour up to almost 500 MPa after which one of the gauges started to exhibit tensile strain whereas the other diametrically opposite gauge showed increasing compressive strains. The shift in the strain readings in one of the gauges occurred at a compressive strain of around 13,000 $\mu\epsilon$ while the other gauge reached up to almost 17000 $\mu\epsilon$ before failure. This behaviour is due to the bulging of the split fibres which expanded laterally under the applied compressive load. A different stress-strain behaviour was exhibited by the GFRP bars with $L_u/d_b = 16$ (Figures 10g to 10i). For both attached strain gauges, stress-strain behaviour was linear up to a strain of around 5000 $\mu\epsilon$, which is taken as the proportional stress limit (f_{pp}) and presented as a solid dot. This is then followed by a nonlinear stress-strain behaviour, where one gauge shows significantly increasing compressive strain with a minor increase in the stress while the other gauge starts to shift from compressive to tensile strain. The proportional stress limit f_{pp} is the starting point of buckling failure, which decreased with the increase in bar diameter from 431 MPa to 226 MPa and 201 MPa for #3, #5, and #6 diameter bars, respectively. The maximum measured axial strain in compression (ϵ_{uc}) is 17110 $\mu\epsilon$ for the tested GFRP bars which represents 81.4% of their ultimate tensile

strain value (ϵ_u). Interestingly, even #3 bars with L_u/d_b ratio of 4 and 8 which recorded f_{fc} values equal to f_{fu} , ϵ_{uc} was 19% less than their ultimate strain value (ϵ_u).

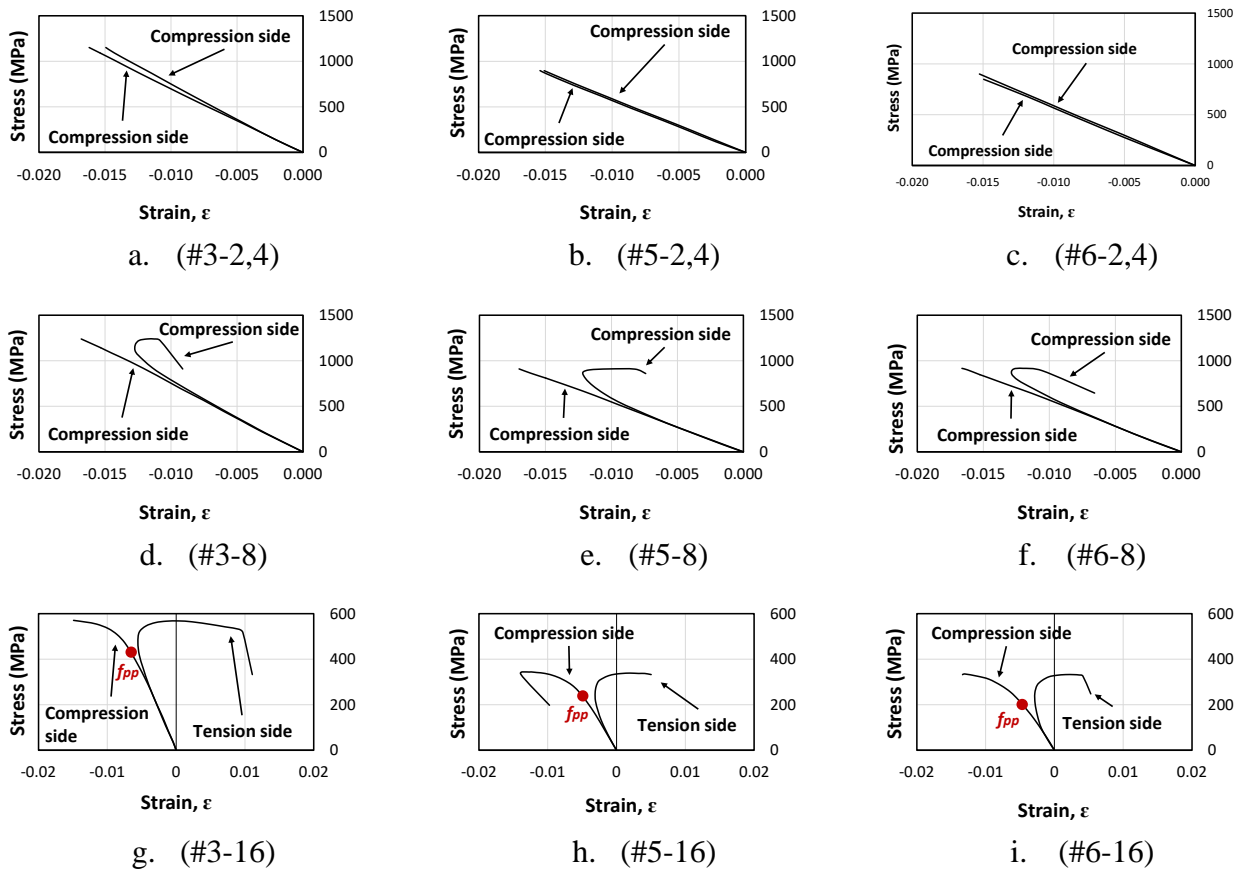


Figure 10. Typical stress-strain behaviour of the tested GFRP bars with different L_u/d_b ratio

The compressive modulus of elasticity (E_{fc}) was calculated as the slope of the linear elastic part of the stress and strain curve and reported in Table 5. Similar to the approach suggested by CSA S806 [34] and ASTM D7205/D7205M [39] to determine the tensile modulus of elasticity of GFRP bars, the E_{fc} values of GFRP bars were measured from the slope of the linear lines between $1000 \mu\epsilon$ and $3000 \mu\epsilon$. The E_{fc} was calculated for both strain readings obtained from the gages on both sides of the tested GFRP bars. As reported in Table 5, very close E_{fc} values were obtained for #5 and #6 bars compared to E_{fu} values, while #3 bars show 12% higher E_{fc} values than E_{fu} values. Moreover, #3 bars showed a slightly higher standard

deviation (SD) and coefficient of variation (CoV) of the test results compared to #5 and #6 GFRP bars.

Table 5. Compressive modulus of elasticity (E_{fc}) (MPa) of the tested GFRP bars with various L_u/d_b ratio

Bar number	No. of strain gauge	#3 (9.5 mm) bar L_u/d_b ratio				#5 (15.9 mm) bar L_u/d_b ratio				#6 (19.1 mm) bar L_u/d_b ratio			
		2	4	8	16	2	4	8	16	2	4	8	16
5	1	71702	72587	77091	68716	58845	60768	61173	58421	59798	60523	61912	62133
	2	72462	70159	75219	70108	61750	61573	59946	56704	60058	57360	60125	59941
6	3	66191	68841	64573	68357	62584	58934	59286	59377	62740	61298	58286	58791
	4	66902	67756	70198	71783	66548	59940	59205	58802	61932	59789	56785	59480
Average		69314	69836	71770	69741	62432	60304	59903	58326	61132	59743	59277	60086
Average all		70165				60241				60059			
SD		2792	1802	4860	1348	2752	979	788	996	1241	1475	1927	1251
CoV (%)		4.0	2.6	6.8	1.9	4.4	1.6	1.3	1.7	2.0	2.5	3.3	2.1
$(E_{fc}/E_{fu})\times 100$		110.9	111.7	114.8	111.6	104.1	100.5	99.8	97.2	101.0	98.7	98.0	99.3

DISCUSSION

The effect of the test parameters was determined by analysing the test data with IBM Statistical Package for the Social Sciences (SPSS) Statistics 23.0 (2015) to compare the significance of the difference of the measured f_{fc} of GFRP bars at a 95% confidence interval. One-way analysis of variance (ANOVA) was used to determine whether there were any significant differences between the f_{fc} measured among the tested bars with different bar diameters and L_u/d_b ratios.

The Influence of Bar Diameter

The bar diameter was found to have no influence on the failure mode of the GFRP bars with the same L_u/d_b ratio. For bars with L_u/d_b ratio of 2 and 4, all the bars failed by crushing whereas the bars with L_u/d_b ratio of 16 failed by buckling and those with L_u/d_b ratio of 8 failed by a combination of crushing and buckling. However, bar diameter was found to affect

the shape of the failure surface in crushing mode of failure only (L_u/d_b ratio of 2 and 4). It was observed that increasing the bar diameter resulted in the uneven micro-fibre buckling inside the bars (Figure 9d), due to the higher shear lag effect in bigger than smaller diameter bars. As also observed in GFRP bars under tension, there is a non-uniform stress distribution (shear lag) through the bars' cross-section wherein a higher stress is experienced by the outer fibres compared to the fibres at the centre of the bar [46].

There was a statistically significant difference between groups of the measured f_{fc} values for all the bar diameters in all L_u/d_b ratios ($p = 0.000$) considered except for $L_u/d_b = 2$ ($p = 0.883$) as determined by one-way ANOVA, as shown in Table 6. The post-hoc Tukey's HSD test in Table 7 reveals that there was no statistically significance difference between the average f_{fc} values for #3, #5 and #6 GFRP bars when $L_u/d_b = 2$. On the other hand, there was statistically significant difference on the average f_{fc} between #3 and #5 bars when the L_u/d_b ratio is 4 to 16, with the #3 bars yielding significantly higher average f_{fc} . On the contrary, the average f_{fc} between #5 and #6 bars is statistically the same. Accordingly, the crushing strength of #3 bars with L_u/d_b ratio = 8 was 50.1% and 59.2% higher than #5 and #6 bars. Moreover, #3 bar with L_u/d_b ratio = 16 showed 54.5% and 68.3% higher buckling stress and 90.3% and 113.9% higher proportional stress limit compared to #5 and #6 bars, respectively. However, Figure 11 shows wider variations in the test results for smaller than bigger diameter bars with L_u/d_b ratio of 2 and 4. This can be attributed to the size effect on the small samples [47-49] evidenced by the increase of stability and convergence in test results for bigger diameter bar with the same L_u/d_b ratio. This can be also observed in Table 4 by the general increase in SD and CoV values with the decrease in bar diameter regardless of L_u/d_b ratios. Moreover, Figure 11 shows that adopting the new test method results in higher compressive-to-tensile strength ratio compared to average test results using the previous testing methodologies [14, 30].

The compressive modulus of elasticity (E_{fc}) reported in Table 5 is almost similar to the tensile modulus of elasticity E_{fu} for #5 and #6 GFRP bars but 12% higher for #3 bars. This higher E_{fc} than E_{fu} for small diameter bar was due to the full engagement of all fibres within the cross-section of the bar which provided equal resistance against the applied load. This observation is also supported by the higher compressive strength of smaller than bigger diameter bars as also observed in the GFRP-reinforced concrete columns reinforced with different bar diameters but with the same reinforcement ratio [3]. Thus, it can be suggested that smaller bar diameters are more preferable than bigger diameter bars as longitudinal reinforcement in concrete columns as they are more effective in resisting applied compressive loads.

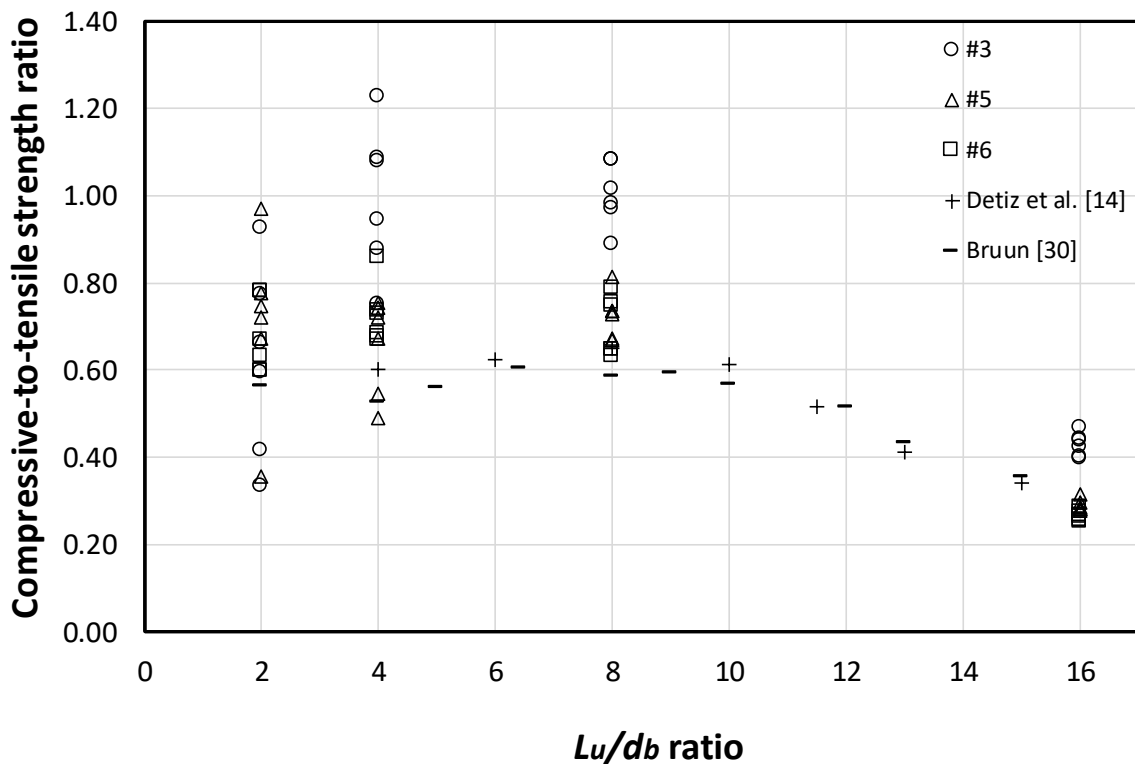


Figure 11. Compressive strength vs L_u/d_b ratio of the tested GFRP bars

Table 6. One-way ANOVA on f_{fc} of GFRP bars with different bar diameters

Description	Sum of Squares	df	Mean Square	F	Sig.
-------------	----------------	----	-------------	---	------

$L_u/d_b = 2$					
Between groups	13093.1	2	6546.5	0.125	0.883
Within groups	783681.2	15	52245.4		
Total	796774.4	17			
$L_u/d_b = 4$					
Between groups	817865.9	2	408932.9	15.9	0.000
Within groups	384193.1	15	25612.8		
Total	1202059.0	17			
$L_u/d_b = 8$					
Between groups	874130.8	2	437065.4	20.6	0.000
Within groups	317980.7	15	21198.7		
Total	1192111.6	17			
$L_u/d_b = 16$					
Between groups	181198.1	2	90599.0	78.1	0.000
Within groups	17383.5	15	1158.9		
Total	198581.6	17			

Table 7. Multiple comparisons on f_{fc} of GFRP bars with different bar diameters

Bar	Bar	Mean Difference	Std. Error	Sig.	95% Confidence Interval	
					Lower Bound	Upper Bound
$L_u/d_b = 2$						
#3	#5	-63.4	131.9	0.881	-406.2	279.3
	#6	-47.6	131.9	0.931	-390.3	295.1
#5	#3	63.4	131.9	0.881	-279.3	406.2
	#6	15.8	131.9	0.992	-326.9	358.6
#6	#3	47.6	131.9	0.931	-295.1	390.3
	#5	-15.8	131.9	0.992	-358.6	326.9
$L_u/d_b = 4$						
#3	#5	497.2	92.3	0.000	257.2	737.2
	#6	386.5	92.3	0.002	146.5	626.5
#5	#3	-497.2	92.3	0.000	-737.2	-257.2
	#6	-110.7	92.3	0.472	-350.7	129.3
#6	#3	-386.5	92.3	0.002	-626.5	-146.5
	#5	110.7	92.3	0.472	-129.3	350.7
$L_u/d_b = 8$						
#3	#5	440.4	84.1	0.000	222.1	658.7
	#6	490.5	84.1	0.000	272.1	708.8
#5	#3	-440.4	84.1	0.000	-658.7	-222.1
	#6	50.1	84.1	0.824	-168.2	268.4
#6	#3	-490.5	84.1	0.000	-708.8	-272.1
	#5	-50.1	84.1	0.824	-268.4	168.2
$L_u/d_b = 16$						
#3	#5	201.9	19.6	0.000	150.8	253.0
	#6	222.2	19.6	0.000	171.2	273.3
#5	#3	-201.9	19.6	0.000	-253.0	-150.8
	#6	20.3	19.6	0.568	-30.7	71.3
#6	#3	-222.2	19.6	0.000	-273.3	-171.2
	#5	-20.3	19.6	0.568	-71.3	30.7

Influence of Slenderness Ratio (L_u/d_b)

The slenderness ratio affected significantly the failure behaviour of GFRP bars in compression. For all bar numbers (#3, #5 and #6), the increase of L_u/d_b ratio from 2 to 16 changed the failure mode from crushing to buckling due to the increase in the unbraced length. In fact, the bars with low L_u/d_b ratios (2 and 4) are prone to shear failure as demonstrated by bar kinking due to the size effect. On the other hand, the bars with L_u/d_b of 8 will exhibit a compression

failure due to lateral expansion of the bars leading to splitting between fibre bundles, which is the typical mode of failure for longitudinal reinforcement in concrete columns. However, the geometric property was dominant for GFRP bars with $L_u/d_b = 16$ [47-49], and all the bars failed by buckling.

As shown in Table 8, there was a statistically significant difference between the measured f_{fc} between groups ($p = 0.000$) for all bar diameters investigated as determined by one-way ANOVA. The post-hoc Tukey's HSD test in Table 9 reveals that the average f_{fc} for #3 bars with L_u/d_b ratio of 2 is statistically significantly lower than the bars with L_u/d_b ratio of 4 and 8 but statistically similar to the bars with L_u/d_b ratio of 16. There was no statistically significant difference between bars with L_u/d_b of 4 and 8 ($p = 1.000$). For #5 bars, the average f_{fc} for bars with L_u/d_b ratio of 2, 4 and 8 is statistically similar to each other but those bars with L_u/d_b ratio of 16 is significantly low. Neither were there any statistically significant differences between f_{fc} for #6 bars with L_u/d_b of 2, 4 and 8, however, f_{fc} measured significantly lower for bars with L_u/d_b ratio of 16. The size effect was responsible for the higher f_{fc} values for #3 and #5 bars as L_u/d_b ratio increased from 2 to 4 and 8, while it was almost equal for #6 bars. The size effect reduced with the increase in L_u/d_b ratio as shown by the low SD and CoV values in Table 4. Accordingly, the GFRP bars with L_u/d_b ratio = 8 recorded the most consistent failure behaviour and the highest f_{fc} values among the tested GFRP bars. With the increase of L_u/d_b ratio from 8 to 16, a 58.8% reduction in f_{fc} value was noticed for all tested bar diameters due to the governing fibre buckling mode of failure (see Figure 11 and Table 4). At high L_u/d_b ratios, the GFRP bars will exhibit a non-linear behaviour and low failure stress due to the elastic buckling effect. From Figure 10, the proportional stress limit (f_{pp}) for slender bars is only 76.4%, 69.0%, and 59.9% of the ultimate buckling stress of #3, #5, and #6 GFRP bars, respectively. Based on Table 4, it can be said that L_u/d_b ratio has no significant influence

on compressive modulus of elasticity (E_{fc}) as this property is measured in the linear elastic region of the stress-strain curve.

Table 8. One-way ANOVA on f_{fc} of GFRP bars with different L_u/d_b ratios

<i>Description</i>	<i>Sum of Squares</i>	<i>df</i>	<i>Mean Square</i>	<i>F</i>	<i>Sig.</i>
#3 bars					
Between groups	2559391.1	3	853130.3	23.4	0.000
Within groups	728860.0	20	36443.0		
Total	3288251.1	23			
#5 bars					
Between groups	1132116.8	3	377372.2	17.3	0.000
Within groups	434794.0	20	21739.7		
Total	1566910.8	23			
#6 bars					
Between groups	1304108.7	3	434702.9	25.6	0.000
Within groups	339584.6	20	16979.2		
Total	1643693.3	23			

Table 9. Multiple comparisons on f_{fc} of GFRP bars with different L_u/d_b ratios

L_u/d_b	L_u/d_b	Mean Difference	Std. Error	Sig.	95% Confidence Interval	
					Lower Bound	Upper Bound
#3 bars						
2	4	-496.0	110.2	0.001	-804.5	-187.5
	8	-507.9	110.2	0.001	-816.4	-199.4
	16	252.3	110.2	0.134	-56.1	560.8
4	2	496.0	110.2	0.001	187.5	804.5
	8	-11.9	110.2	1.000	-320.3	296.5
	16	748.4	110.2	0.000	439.9	1056.9
8	2	507.9	110.2	0.001	199.4	816.4
	4	11.9	110.2	1.000	-296.5	320.3
	16	760.3	110.2	0.000	451.8	1068.8
16	2	-252.3	110.2	0.134	-560.8	56.1
	4	-748.4	110.2	0.000	-1056.9	-439.9
	8	-760.3	110.2	0.000	-1068.8	-451.8
#5 bars						
2	4	64.6	85.1	0.872	-173.6	302.9
	8	-4.0	85.1	1.000	-242.3	234.1
	16	517.8	85.1	0.000	279.5	756.0
4	2	-64.6	85.1	0.872	-302.9	173.6
	8	-68.7	85.1	0.850	-306.9	169.5
	16	453.1	85.1	0.000	214.8	691.4
8	2	4.0	85.1	1.000	-234.1	242.3
	4	68.7	85.1	0.850	-169.5	306.9
	16	521.8	85.1	0.000	283.6	760.1
16	2	-517.8	85.1	0.000	-756.0	-279.5
	4	-453.1	85.1	0.000	-691.4	-214.8
	8	-521.8	85.1	0.000	-760.1	-283.6
#6 bars						
2	4	-61.9	75.2	0.843	-272.4675	148.6675
	8	30.1	75.2	0.978	-180.4175	240.7175
	16	522.2	75.2	0.000	311.6991	732.8342
4	2	61.9	75.2	0.843	-148.6675	272.4675
	8	92.0	75.2	0.620	-118.5175	302.6175
	16	584.1	75.2	0.000	373.5991	794.7342
8	2	-30.1	75.2	0.978	-240.7175	180.4175
	4	-92.0	75.2	0.620	-302.6175	118.5175
	16	492.1	75.2	0.000	281.5491	702.6842
16	2	-522.2	75.2	0.000	-732.8342	-311.6991
	4	-584.1	75.2	0.000	-794.7342	-373.5991
	8	-492.1	75.2	0.000	-702.6842	-281.5491

Reliability of the New Compressive Test Method for GFRP Bars

The reliability of the new compressive test method was evaluated by statistically analysing the test results using the SPSS and comparing the test results to those from previous studies which used different test methods. The provision of steel caps filled with grout in the top and bottom portion of the GFRP bars enabled the specimen to be placed longitudinally upright in the equipment and facilitated the application of concentric compressive load. There were no signs of eccentricity induced bending moment effects which indicates the suitability of the fabrication process. This can be demonstrated by the nearly equal strain readings on gauges attached on two sides of the test specimens in the linear elastic region of the stress-strain curve. Except for bars with L_u/d_b ratio of 2, there was no observed premature failure in tested specimens caused by the high stress concentration at the top and bottom of the bars. This provided a consistent failure behaviour and statistically similar compressive strength value between the test groups.

The reliability of the test method was further verified after comparing the test results with the previous studies as shown in Figure 11. This figure shows that the new compression test method generally yields higher and more consistent compressive-to-tensile strength ratio when compared to other previous test results [14, 30]. More noticeably, the significant enhancement in the compressive behaviour of the GFRP bars using the new test method occurred with the bars exhibiting crushing and splitting failure, while the compressive-to-tensile strength ratio was almost similar under the effect of buckling. This finding indicates that the compressive strength obtained from the crushing and splitting modes of failure is significantly affected by the test method. By using the proposed new test method, any premature and unacceptable failure due to the effect of the test setup can be eliminated to obtain test results that accurately and reliably describe the compressive behaviour and strength capacity of the GFRP bars. Based on the test results and statistical analysis, it was found that

the most representative value for the compressive strength of GFRP bars is the one induced by using L_u/d_b ratio of 8. Therefore, this L_u/d_b ratio is recommended for testing GFRP bars in compression to achieve consistent and reliable test results. Consequently, these findings emphasize the high reproducibility of test results using the proposed test methodology for determining the compressive behaviour of GFRP bars with different bar diameters and L_u/d_b ratios.

EVALUATION OF COMPRESSIVE PROPERTIES OF GFRP BARS

Crushing Strength of GFRP Bars

The crushing strength f_{fc} of the GFRP bars was determined from the bars tested with L_u/d_b ratio of 8 or less. As shown in Figure 12, the crushing compressive strength is affected by the nominal area of the bars (A_G). The #3 bars have f_{fc} values almost equal to tensile f_{fu} values whereas the #5 and #6 bars have 27% and 30% lower f_{fc} values than their corresponding f_{fu} values, respectively. Thus, a correlation factor is determined from the equation of the power line that best describes the relationship between the reduction factor, α and the cross sectional area (A_G) curve. This factor accounts for the difference in the ratio of the compressive strength to that of the tensile strength by considering the nominal area of the GFRP bars as proposed in Eq. (1). Comparing to the most recent study [37], close prediction for α with a difference of 3% can be found only for 15.9 mm bar diameter. However, the same study 35% underestimates and 21% overestimates α factor for 12.7 mm and 19.1 mm bar diameter, respectively. This can be due to the premature failure inside the caps and also due to consider one slenderness ratio of 2.

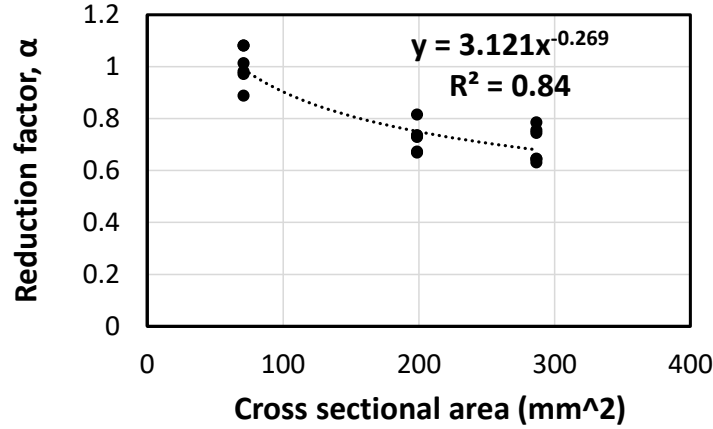


Figure 12. Reduction factor (α) applied for f_{fc} versus cross-section area (A_G) of the bars

$$f_{fc} = \alpha f_{fu} = 3.12 f_{fu} / (A_G)^{0.27} \quad \text{Eq. (1)}$$

Buckling Stress

Euler formula, shown in Eq.(2) is the most common equation used for estimating the elastic buckling load of homogenous material. In this relation, E_{fc} is the compressive modulus of elasticity of the material, and $\frac{kl}{r}$ is the slenderness ratio. This equation was modified to account for the non-homogenous nature of the GFRP bars. It should be mentioned that GFRP bars with $L_u/d_b = 16$ will have an $\frac{l}{r}$ ratio of 32. For #5 and #6 GFRP bars tested in this study, experimentally measured value of 60.0 GPa was used for E_{fc} while an average value of 68.0 GPa was used for #3 bars (Table 5). The results showed a high variation between the experimental (f_{fc-b}) and theoretical (F_{b-eu}) buckling stresses, as reported in Table 10 and the triangular data points in Figure 13(b). Note that the k factor in Eq. (2) is assumed to be 1.0. This assumption is supported by the ability of the upper load platen to allow some rotation in the samples during testing. A reduction factor (β) (Eq. (3)) was suggested to account for the relationship of the ratio of proportional stress limit and the maximum buckling stress to that of the moment of inertia of the bars, I_g (see Figure 13(a)). The nominal bar diameter was used in the calculation of the I_g . The calibration factor was then applied to Eq. (3) leading to the

modified Euler equation (Eq. (4)). The prediction showed a good agreement between f_{fc-b} and F_{b-th} as demonstrated by the circular data points in Figure 13(b) with a deviation of $\pm 15\%$ indicating that the modified Euler equation can provide an improved and reliable estimation for the buckling strength of GFRP bars. Applying this equation to a previous study done by Detiz et al. [14], which considered the slenderness ratio one of the main parameters, resulted in 43% overestimation for their experimental results which might be referred to the difference in fibre content amount.

$$F_{b-eu} = \frac{\pi^2 E_{fc}}{\left(\frac{kl}{r}\right)^2} \quad \text{Eq. (2)}$$

$$\beta = \frac{3(l_g)}{10000} + 0.775 \quad \text{Eq. (3)}$$

$$F_{b-th} = \beta(F_{b-eu}) \quad \text{Eq. (4)}$$

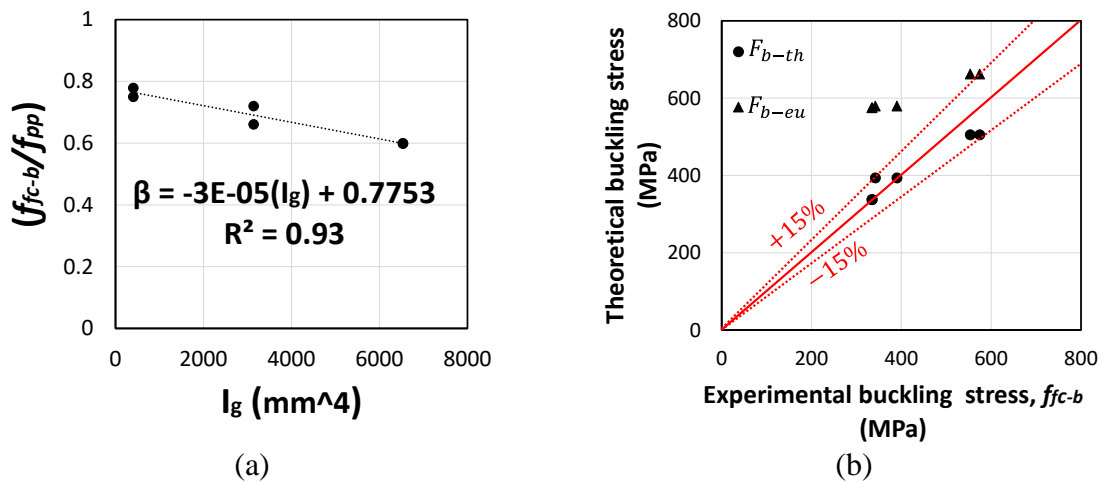


Figure 13. (a) Reduction factor β (b) comparison between experimental and theoretical buckling stress results

Table 10. Comparison between experimental and theoretical buckling stresses

Bar grade	Bar number	Experimental E_{fc} (MPa)	Adopted E_{fc} (MPa)	f_{fc-b} (MPa)	f_{pp} (MPa)	F_{b-eu} (MPa)	$\frac{F_{b-eu}}{F_{b-ex}}$	F_{b-th} (MPa)	$\frac{F_{b-th}}{F_{b-ex}}$
#3	5	69412	69000	553.3	431.0	662.3	1.21	505.5	0.92
	6	70070		574.4	431.0		1.17		0.88
#5	5	57563	57000	390.2	281.0	578.3	1.42	393.9	0.96
	6	57590		342.0	226.0		1.62		1.09

#6	5	61037	59000	334.0	200.0	583.1	1.73	337.8	1.00
	6	59136		335.1	201.0		1.73		1.00

Compressive Behaviour of GFRP Bars

It was considered in this study that L_u/d_b ratio of 8 will provide a good representation of the compressive strength (f_{fc}) for high modulus GFRP bars (Eq. (1)). For L_u/d_b ratio greater than 8, a linear descending line is proposed to represent the strength reduction due to buckling effect. A simplified relation and conservative approach was proposed by adopting the steepest descending line, which is related to the #3 bars. Based on that approach, Figure 14 shows the compressive-to-tensile strength (f_{fc}/f_{fu}) ratio for different GFRP bar diameters with respect to L_u/d_b ratios. For GFRP bars with L_u/d_b ratio less than or equal 8, the prediction equation for f_{fc} is adopted from Eq. (1). When L_u/d_b ratio is more than 8, a reduction should be applied as per the proposed function in Eq. (5) which is graphically presented in Figure 14. From these results, it is recommended that a clear spacing of the spiral or lateral ties for longitudinal reinforcements in compression should be specified at a maximum value of $8d_b$ to effectively utilise the high strength of GFRP bars. This is in contrast with the suggested specification by the CSA S806 code [34] (clause 8.4.3.13) to provide a maximum spiral or tie spacing of 75 mm between lateral reinforcements under compression. While this CSA spacing specification is appropriate for small bar diameter bars, this is very conservative for bigger bar diameters as found in this study. More importantly, the compressive behaviour of GFRP bars evaluated and modeled in this study increases the confidence in accounting for their contribution in the determination of axial load capacity of reinforced concrete columns.

$$f_{fc}(MPa) = \left\{ \begin{array}{ll} 3.1f_{fu}/(A_G)^{0.27}, & L_u/d_b \leq 8 \\ (3.1f_{fu}/(A_G)^{0.27}) - 93(L_u/d_b - 8), & L_u/d_b > 8 \end{array} \right\} \quad \text{Eq. (5)}$$

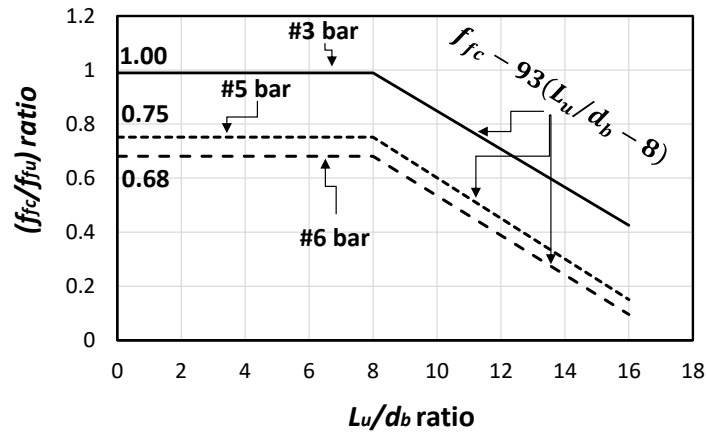


Figure 14. Compressive behaviour of GFRP bars with L_u/d_b ratio

CONCLUSIONS

This study comprehensively and systematically investigated the effect of bar diameter and the unbraced length-to-bar diameter ratio (L_u/d_b) on the compressive behaviour of high-modulus GFRP bars. A new method was also implemented to test the GFRP bars in compression. Theoretical models have been proposed to predict the compressive strength of GFRP bars at different L_u/d_b ratios. Based on the findings and observations, the following conclusion can be drawn:

- The proposed method of testing the GFRP bars under compression gave a reliable and consistent compressive strength of high modulus GFRP bars. This approach facilitated longitudinally upright placement of the specimens and concentric application of the compressive loads without causing eccentricity-related bending effects. Except for bars with L_u/d_b ratio of 2, there was no observed premature failure in tested bars due to high stress concentration at the top and bottom portion of the bars.
- Bars with an L_u/d_b ratio of 8 gave the most representative value for the compressive strength and elastic modulus, and is recommended for testing high modulus GFRP bars in compression to achieve consistent and reliable results. The GFRP bars with this L_u/d_b ratio failed by longitudinal splitting along the fibre length and damage in the

matrix, which represents closely the failure behaviour in compression of the longitudinal bars in concrete columns.

- The bar diameter has no influence on the failure mode of the GFRP bars with the same L_u/d_b ratio. Bars with L_u/d_b ratio up to 4 failed by crushing, higher than a ratio of 8 failed by buckling, and those within a ratio of 4 to 8 failed by a combination of crushing and buckling.
- There was a statistically significant difference between groups of the measured compressive strength of GFRP bars with different bar diameters. For GFRP bars with L_u/d_b greater than 2, the average compressive strength of #3 bars is significantly higher than the #5 and #6 bars. This can be attributed to the size effects where most if not all of the fibers in small diameter bars carry the load uniformly throughout its cross-section, but the outermost fibers are stressed more than the inner fibers in bigger diameter bars. This also explains the higher compressive modulus of elasticity of #3 bars than the #5 and #6 GFRP bars.
- Smaller diameter bars are more effective in resisting compressive loads than the bigger diameter bars. The #3 GFRP bars exhibited 50.1% and 59.2% higher crushing strength, 54.5% and 68.3% higher buckling strength, and 90.3% and 113.9% higher proportional stress limit than #5 and #6 GFRP bars, respectively. The smaller #3 diameter bars also provided almost similar strength in tension whereas the #5 and #6 bars failed at a compressive stress of only 75% and 65%, respectively of their tensile strength.
- The slenderness ratio affected significantly the failure behaviour and load capacity of GFRP bars in compression but had no significant influence on the compressive modulus of elasticity. For all bar diameters, the increase in L_u/d_b ratio from 2 to 16 changed the failure mode from crushing to buckling due to an increase in the unbraced length. In general, the compressive strength of GFRP bars is statistically significantly higher for

bars with L_u/d_b ratio of 2 to 8 than those bars with L_u/d_b ratio of 16. However, the standard deviation and coefficient of variation of the test results of the compressive strength is higher for GFRP bars with lower L_u/d_b ratios.

- Empirical equation accounting for the nominal bar diameter (or area) and considering a reduction factor that accounts for the difference in bar diameter was proposed to predict the compressive crushing strength of the GFRP bars. In addition, a modified Euler equation accounting for the unbraced length-to-bar diameter ratio and non-homogenous properties of slender GFRP bars was proposed to predict the buckling strength.

The results of this study provide a better understanding of the compressive behaviour of GFRP bars. It is suggested however that the reliability of the proposed new test method should be further calibrated for other types of FRP reinforcements with different bar diameters. Moreover, the size of the steel pipes can be optimised by further attempts. Nevertheless, the major findings and recommendations made are very helpful for extensively and confidently using high modulus GFRP bars as longitudinal reinforcements in concrete columns, and to account for their contribution in the load capacity prediction of GFRP-reinforced concrete columns.

ACKNOWLEDGEMENTS

The authors are also grateful to Pultrall Canada and Inconmat V-ROD Australia for providing the GFRP bars. The second author acknowledges the scholarship granted by the Australian Government Endeavour Executive Leadership Award to undertake his professional development at the Centre for Integration of Composites into Infrastructure (CICI), West Virginia University, Morgantown, USA. The assistance of the postgraduate students and technical staff at the Centre of Future Materials (CFM) is also acknowledged.

REFERENCES

1. Manalo, A., B. Benmokrane, K.-T. Park, and D. Lutze, *Recent developments on FRP bars as internal reinforcement in concrete structures*. Concrete in Australia, 2014. **40**(2): p. 46-56.
2. Maranan, G., A. Manalo, B. Benmokrane, W. Karunasena, and P. Mendis, *Behavior of concentrically loaded geopolymer-concrete circular columns reinforced longitudinally and transversely with GFRP bars*. Engineering Structures, 2016. **117**: p. 422-436.
3. AlAjarmeh, O.S., A.C. Manalo, B. Benmokrane, W. Karunasena, and P. Mendis, *Axial performance of hollow concrete columns reinforced with GFRP composite bars with different reinforcement ratios*. Composite Structures, 2019b. **213**(1): p. 12.
4. AlAjarmeh, O.S., A. Manalo, B. Benmokrane, W. Karunasena, P. Mendis, and K. Nguyen, *Compressive behavior of axially loaded circular hollow concrete columns reinforced with GFRP bars and spirals*. Construction and Building Materials, 2019a. **194**: p. 12-23.
5. Maranan, G., A. Manalo, B. Benmokrane, W. Karunasena, P. Mendis, and T. Nguyen, *Shear behaviour of geopolymer-concrete beams transversely reinforced with continuous rectangular GFRP composite spirals*. Composite Structures, 2018. **187**: p. 454-465.
6. El-Nemr, A., E.A. Ahmed, and B. Benmokrane, *Flexural Behavior and Serviceability of Normal-and High-Strength Concrete Beams Reinforced with Glass Fiber-Reinforced Polymer Bars*. ACI structural journal, 2013. **110**(6).
7. Maranan, G., A. Manalo, K. Karunasena, and B. Benmokrane, *Bond stress-slip behavior: case of GFRP bars in geopolymer concrete*. Journal of Materials in Civil Engineering, 2014. **27**(1): p. 04014116.
8. Maranan, G., A. Manalo, W. Karunasena, B. Benmokrane, and D. Lutze, *Flexural behaviour of glass fibre reinforced polymer (GFRP) bars subjected to elevated temperature*. 2014.
9. Maranan, G., A. Manalo, W. Karunasena, and B. Benmokrane, *Pullout behaviour of GFRP bars with anchor head in geopolymer concrete*. composite structures, 2015. **132**: p. 1113-1121.
10. Benmokrane, B., H.M. Mohamed, A. Manalo, and P. Cousin, *Evaluation of physical and durability characteristics of new headed glass fiber-reinforced polymer bars for concrete structures*. Journal of Composites for Construction, 2016. **21**(2): p. 04016081.
11. Benmokrane, B., A.H. Ali, H.M. Mohamed, A. ElSafty, and A. Manalo, *Laboratory assessment and durability performance of vinyl-ester, polyester, and epoxy glass-FRP bars for concrete structures*. Composites Part B: Engineering, 2017. **114**: p. 163-174.
12. Benmokrane, B., C. Nazair, X. Seynave, and A. Manalo, *Comparison between ASTM D7205 and CSA S806 Tensile-Testing Methods for Glass Fiber-Reinforced Polymer Bars*. Journal of Composites for Construction, 2017. **21**(5): p. 04017038.
13. Nazair, C., B. Benmokrane, M.-A. Loranger, M. Robert, and A. Manalo, *A comparative study of the thermophysical and mechanical properties of the glass fiber reinforced polymer bars with different cure ratios*. Journal of Composite Materials, 2018: p. 0021998318774833.

14. Deitz, D., I. Harik, and H. Gesund, *Physical properties of glass fiber reinforced polymer rebars in compression*. Journal of Composites for Construction, 2003. **7**(4): p. 363-366.
15. Benmokrane, B., A. Manalo, J.-C. Bouhet, K. Mohamed, and M. Robert, *Effects of Diameter on the Durability of Glass Fiber-Reinforced Polymer Bars Conditioned in Alkaline Solution*. Journal of Composites for Construction, 2017. **21**(5): p. 04017040.
16. Benmokrane, B., C. Nazair, M.-A. Loranger, and A. Manalo, *Field Durability Study of Vinyl-Ester-Based GFRP Rebars in Concrete Bridge Barriers*. Journal of Bridge Engineering, 2018. **23**(12): p. 04018094.
17. Davalos, J.F., Y. Chen, and I. Ray, *Long-term durability prediction models for GFRP bars in concrete environment*. Journal of Composite Materials, 2012. **46**(16): p. 1899-1914.
18. Robert, M. and B. Benmokrane, *Behavior of GFRP reinforcing bars subjected to extreme temperatures*. Journal of Composites for Construction, 2009. **14**(4): p. 353-360.
19. 807-15, C., *Specifications for fibre-reinforced polymers*. Canadian Standards Authority (CSA), 2015.
20. DTMR-2018, SD4003 - *Precast planks for boat ramp - Type RG4000 FRP*. Queensland Department of Transport and Main Roads, Brisbane, Queensland, 2018.
21. Benmokrane, B., M. Eisa, S. El-Gamal, E. El-Salakawy, and D. Thebeau. *First use of GFRP bars as reinforcement for continuous reinforced concrete pavement*. in *Proceedings of the 4th International Conference on FRP Composites in Civil Engineering (CICE2008), Zurich, Switzerland*. 2008.
22. Standardization, I.O.f., *ISO 10406-1: 2015: Fibre-Reinforced Polymer (FRP) Reinforcement of Concrete: Test Methods: Part 1: FRP Bars and Grids*. 2015, ISO Geneva.
23. D7957M-17, A.D., *Standard Specification for Solid Round Glass Fiber Reinforced Polymer Bars for Concrete Reinforcement*. ASTM International, West Conshohocken, PA, 2017.
24. ASTM D695-10, *Standard Test Method for Compressive Properties of Rigid Plastics*. ASTM International, West Conshohocken, PA, 2010.
25. No.3, I.D.M., *Reinforcing Concrete Structures with Fibre Reinforced Polymers*. Intelligent Sensing for Innovative Structures Canada, Winnipeg, 2001.
26. Khan, Q.S., M.N. Sheikh, and M.N. Hadi, *Tension and compression testing of fibre reinforced polymer (FRP) bars*. 2015.
27. Khorramian, K. and P. Sadeghian. *New Testing Method of GFRP Bars in Compression*. in *CSCCE Annual Conference 2018, Fredericton, NB, Canada*. 2018. Canadian Society for Civil Engineering.
28. Chaallal, O. and B. Benmokrane, *Physical and mechanical performance of an innovative glass-fiber-reinforced plastic rod for concrete and grouted anchorages*. Canadian Journal of Civil Engineering, 1993. **20**(2): p. 254-268.
29. Robert, M. and B. Benmokrane, *Physical, mechanical, and durability characterization of preloaded GFRP reinforcing bars*. Journal of Composites for Construction, 2010. **14**(4): p. 368-375.
30. Bruun, E., *GFRP bars in structural design: determining the compressive strength versus unbraced length interaction curve*. Canadian Young Scientist Journal, 2014. **3**(1): p. 22-29.

31. Deitz, D., I.E. Harik, and H. Gesund, *GFRP reinforced concrete bridge decks*. 2000, University of Kentucky Transportation Center.
32. Khorramian, K. and P. Sadeghian, *Experimental and analytical behavior of short concrete columns reinforced with GFRP bars under eccentric loading*. *Engineering Structures*, 2017. **151**: p. 761-773.
33. Fillmore, B. and P. Sadeghian, *Contribution of longitudinal glass fiber-reinforced polymer bars in concrete cylinders under axial compression*. *Canadian Journal of Civil Engineering*, 2018. **45**(6): p. 458-468.
34. CSA, *Design and construction of building structures with fibre-reinforced polymers*. 2012: Canadian Standards Association, CAN/CSA-S806-12, Rexdale, ON, Canada.
35. ASTM D3171-15, *Standard test methods for constituent content of composite materials*. ASTM D3171-15, West Conshohocken, PA, 2015.
36. ACI, *Guide for the Design and Construction of Concrete Reinforced with FRP Bars (440.1R-15)*. American Concrete Institute, Farmington Hills, MI, 2015.
37. Sadeghian, P. and K. Khorramian, *Material Characterization of GFRP Bars in Compression Using a New Test Method*. *Journal of Testing and Evaluation*, 2019. **49**(2).
38. Manalo, A., H. Mutsuyoshi, and T. Matsui, *Testing and characterization of thick hybrid fibre composites laminates*. *International Journal of Mechanical Sciences*, 2012. **63**(1): p. 99-109.
39. ASTM D7205/D7205M-06, *Standard Test Method for Tensile Properties of Fiber Reinforced Polymer Matrix Composite Bars*. ASTM International, West Conshohocken, PA, 2016.
40. Papia, M., G. Russo, and G. Zingone, *Instability of longitudinal bars in RC columns*. *Journal of Structural Engineering*, 1988. **114**(2): p. 445-461.
41. Mau, S. and M. El-Mabsout, *Inelastic buckling of reinforcing bars*. *Journal of Engineering Mechanics*, 1989. **115**(1): p. 1-17.
42. Mau, S., *Effect of tie spacing on inelastic buckling of reinforcing bars*. *Structural Journal*, 1990. **87**(6): p. 671-677.
43. Bae, S., A.M. Miseses, and O. Bayrak, *Inelastic buckling of reinforcing bars*. *Journal of Structural Engineering*, 2005. **131**(2): p. 314-321.
44. S807-10, C.C., *Specification for fibre reinforced polymers*. Rexdale, Ontario, Canada, 2010.
45. Afifi, M.Z., H.M. Mohamed, and B. Benmokrane, *Axial capacity of circular concrete columns reinforced with GFRP bars and spirals*. *Journal of Composites for Construction*, 2013. **18**(1).
46. Bank, L.C., *Composites for construction: structural design with FRP materials*. 2006: John Wiley & Sons.
47. Atkins, A.G. and R.M. Caddell, *The laws of similitude and crack propagation*. *International Journal of Mechanical Sciences*, 1974. **16**(8): p. 541-548.
48. Mai, Y. and A. Atkins, *Crack propagation in non-proportionally scaled elastic structures*. *International Journal of Mechanical Sciences*, 1978. **20**(7): p. 437-449.
49. Silva, M.A. and C.C. Rodrigues, *Size and relative stiffness effects on compressive failure of concrete columns wrapped with glass FRP*. *Journal of Materials in Civil Engineering*, 2006. **18**(3): p. 334-342.